

Cascades transition in generalised two-dimensional turbulence

Vibhuti Bhushan Jha^{1,2}†, Kannabiran Seshasayanan³‡ and Vassilios Dallas⁴¶

¹Space Applications Centre, Indian Space Research Organisation, Ahmedabad, Gujarat, India

²Department of Physics, Indian Institute of Technology Kharagpur, Kharagpur, West Bengal, India

³Department of Applied Mechanics, Indian Institute of Technology Madras, Chennai, India

⁴Mathematical Institute, University of Oxford, Oxford, OX2 6GG, UK

(Received xx; revised xx; accepted xx)

The generalised two-dimensional (2D) fluid is characterised by a relationship between a scalar field q , called generalised vorticity, and the stream function ψ , namely $q = -(\nabla^2)^{\frac{\alpha}{2}}\psi$. We study the transition of cascades in generalised 2D turbulence by systematically varying the parameter α and investigating its influential role in determining the directionality (inverse, forward, or bidirectional) of these cascades. We identify a finite critical threshold α_c , where a transition occurs in cascade directionality, emphasising that $\alpha = 0$ signifies a laminar flow state with a vanishing nonlinear term. At a critical value of α_c a small wavelength instability is induced in the laminar flow. Using perturbation analysis we obtain that α_c is inversely proportional to the square of the Reynolds number – a scaling validated through numerical simulations. We derive upper bounds for the dimensionless dissipation rates of generalised energy E_G and enstrophy Ω_G as the Reynolds number tends to infinity. These findings corroborate numerical simulations, illustrating the inverse cascade of E_G and forward cascade of Ω_G for $\alpha > 0$, contrasting with the reverse behaviour for $\alpha < 0$. The dependence of dissipation rates on system parameters reinforces these observed transitions, substantiated by spectral fluxes and energy spectra, which hint at Kolmogorov-like scalings at large scales but discrepancies at smaller scales. These discrepancies are possibly due to nonlocal transfers, which dominate the dynamics as we go from positive to negative values of α . Intriguingly, the forward cascade of E_G for $\alpha < 0$ reveals similarities to three-dimensional turbulence, notably the emergence of vortex filaments within a 2D framework, marking a unique feature of this generalised model.

Key words: Keywords

1. Introduction

The presence of nonlinear interactions allow energy to be redistributed across different length scales in turbulent flows. While in three-dimensional (3D) turbulence, energy is distributed to small scales (forward cascade), energy is transferred to large scales in two-

† Email address for correspondence: vibhutibjha@gmail.com

‡ Email address for correspondence: kanna@iitm.ac.in

¶ Email address for correspondence: vassilios.dallas@gmail.com

dimensional (2D) turbulence (inverse cascade). This, along with the existence of other quadratic invariants make 2D turbulence an exciting system. Not entirely limited to theoretical or numerical excursions, such behaviour has been observed in atmospheric (Lilly 1969; Rhines 1979; Nastrom *et al.* 1984; Read 2001) and planetary flows (Siegelman *et al.* 2022). The presence of external mechanisms like rotation, stratification, presence of magnetic field or compactification of a dimension can make the prediction of the cascade direction challenging (Celani *et al.* 2010; Alexakis 2011; Sen *et al.* 2012; Marino *et al.* 2013; Deusebio *et al.* 2014) due to competing behaviour between the forward and inverse cascades, often dependent on some control parameter like anisotropy, rotation rate, etc. This results in bidirectional cascades, which depend on the control parameter. Such bidirectional cascades have been observed in numerical (Smith *et al.* 1996; Alexakis 2011; Seshasayanan *et al.* 2014a; Sozza *et al.* 2015) and experimental settings (Shats *et al.* 2010; Xia *et al.* 2011; Campagne *et al.* 2014). Furthermore, there is evidence for bidirectional cascade in atmospheric (Byrne & Zhang 2013; King *et al.* 2015; Shao *et al.* 2023), oceanic (Scott & Wang 2005; Arbic *et al.* 2013; Balwada *et al.* 2016; Khatri *et al.* 2018) and planetary flows (Lesur & Longaretti 2011; Young & Read 2017).

The transition from one type of cascade to another can be either smooth or at a critical point (Alexakis & Biferale 2022). The presence of a critical dimension at which the cascade direction changes has been demonstrated by Frisch *et al.* (1976). Benavides & Alexakis (2017) found the transition from a forward to a bidirectional cascade in thin layers of fluid turbulence to be critical (Ecke 2017). In 2D magnetohydrodynamic (MHD) turbulence, the variation in magnetic field above a critical value leads to cascade transition (Seshasayanan *et al.* 2014a), and the energy flux scales as a power law. Similarly under certain regimes, MHD flows can behave like a 2D flow at large scales and 3D like at smaller scales (Alexakis 2011). In this case, the inverse cascade of energy is highly sensitive to the strength of the magnetic field.

Pierrehumbert *et al.* (1994a) considered a generalised model of 2D turbulence characterised by a parameter α which links the streamfunction to a scalar field called generalised vorticity. Certain values of α lead to equations relevant in the context of geophysical flows. For $\alpha = 2$ the generalised model gives the familiar barotropic vorticity equation from 2D Navier-Stokes (Tabeling 2002; Boffetta & Ecke 2012). For $\alpha = 1$ it gives the surface quasi-geostrophic (SQG) equation, which describes the motion of a rotating stratified fluid (Held *et al.* 1995; Lapeyre 2017). For $\alpha = -2$ it gives a rescaled shallow-water quasi-geostrophic equation in the asymptotic limit of length scales large compared to the deformation scale (Larichev & McWilliams 1991; Smith *et al.* 2002). In generalised 2D turbulence, changing the value of α leads to varying degrees of forward and inverse cascades. There are various studies using different values of α and analysing the associated energy spectra (Tran 2004; Watanabe & Iwayama 2004a; Iwayama *et al.* 2015).

In the presence of an inverse cascade, strain rate arguments for spectral locality are based on negative eddy viscosity. In other words, the notion that strain thins smaller scale vortices and so energy is transferred toward large scales (Kraichnan 1976). The cascades of 2D Navier-Stokes turbulence ($\alpha = 2$) has been predicted that are less local than of the 3D turbulence (Kraichnan 1971; Boffetta & Ecke 2012). Pierrehumbert *et al.* (1994a) focus on positive values of α only and argue that $\alpha = 2$ is at the transition between local to nonlocal enstrophy transfers, in the sense that dominant straining of small scales comes from the largest scales when $\alpha > 2$. This is confirmed by numerical simulations (Watanabe & Iwayama 2004b). On the other hand, it is argued that the energy transfers become nonlocal when $\alpha > 4$ (Pierrehumbert *et al.* 1994a). However, depending on the dynamics generating an inverse cascade, spectral locality of strain rate may not indicate local transfers (Burgess & Shepherd 2013). On the other hand, Watanabe & Iwayama

(2007); Foussard *et al.* (2017) found nonlocal interactions in the generalised enstrophy transfer for $1 \leq \alpha \leq 2$.

The value of α decides the nature of cascade. For positive α , energy (enstrophy) cascades to large (small) scales whereas energy (enstrophy) cascades to small (large) scales for negative α . Thus, depending on the sign and value of α , the cascade would either be inverse, forward or bidirectional. This suggests that there is some critical α_c at which there is a transition in the direction of the cascades. However, the aforementioned studies did not study systematically the $\alpha < 0$ regime. In this work we focus on the theoretical and numerical study of the cascades in generalised 2D turbulence by systematically varying α from positive to negative values. We use mathematical inequalities to derive bounds on generalised energy and enstrophy dissipation rates and perform DNS to determine the critical point α_c . Finally, our present study deals with the degree of non-locality of triadic interactions for different values of α .

The paper is organised as follows. In section 2 we discuss the problem formulation and details of the model. In section 3 we derive theoretical bounds on the generalised energy and enstrophy dissipation rates. We present numerical results in section 4 and finally we summarise our concluding remarks in section 5.

2. Problem Formulation

Consider the 2D evolution equation of the generalised vorticity $q(x, y, t)$ in a periodic domain

$$\partial_t q + \mathcal{J}(\psi, q) = \nu_+ \nabla^{2n} q + \nu_- \nabla^{-2m} q + f_q \quad (2.1)$$

where $\psi(x, y, t)$ is the streamfunction, the nonlinear term given by the Jacobian $\mathcal{J}(\psi, q) = \partial_x \psi \partial_y q - \partial_y \psi \partial_x q$, ν_+ is the small scale diffusion coefficient, ν_- is the large scale diffusion coefficient and $f_q = -(-\nabla^2)^{\frac{\alpha}{2}} f_\psi$ is the external forcing, where $f_\psi = f_0 \sin(k_f x) \sin(k_f y)$ with f_0 denoting the amplitude of the forcing. The fluid velocity is given by $\mathbf{u} = \nabla \times (\psi \hat{z})$. The generalised relationship between q and ψ in 2D fluid dynamics is,

$$q = -(-\nabla^2)^{\frac{\alpha}{2}} \psi \quad (2.2)$$

as discussed by Pierrehumbert *et al.* (1994b).

In the presence of an inverse cascade the energy of the large-scale modes grow to extreme values forming a condensate, the growth saturates when the viscous dissipation at the largest scale balances the energy injection (Chertkov *et al.* 2007; Boffetta & Ecke 2012). To prevent the formation of a very large condensate and to reach a turbulent stationary regime we supplement our system with a large scale dissipative term $\nu_- \nabla^{-2m} q$ that is responsible for saturating the inverse cascade. Here we consider hypo-viscosity by raising the inverse Laplacian to the power of $m = 2$ and hyper-viscosity by raising the Laplacian of the viscous term $\nu_+ \nabla^{2n} q$ to the power of $n = 2$. The hyper-viscosity models very large Reynolds number flows giving a wider inertial range, as the viscous term kicks in at much smaller scales compared to the normal viscosity case. The hypo-viscosity does the same by extending the inertial range for scales larger than the forcing scale.

We denote the dimensions of a quantity g by using the square bracket $[g]$. Considering the fact that the variables x, y have units of length $[L]$, and t has units of time $[T]$, then $[\psi] = [L]^2 [T]^{-1}$ and $[q] = [L]^{2-\alpha} [T]^{-1}$. So, the two dimensionless parameters are the small scale Reynolds number

$$Re_+ = \sqrt{f_0 k_f} / (\nu_+ k_f^{2n-1/2}), \quad (2.3)$$

and the large scale Reynolds number

$$Re_- = \sqrt{f_0 k_f} / (\nu_- k_f^{-2m-1/2}), \quad (2.4)$$

with $[f_0] = [L]^2 [T]^{-2}$, $[\nu_+] = [L]^{2n} [T]^{-1}$ and $[\nu_-] = [L]^{-2m} [T]^{-1}$.

In the limit of $\nu_+ \rightarrow 0$, $\nu_- \rightarrow 0$ and $f_q = 0$ the integral over a periodic domain of any function of the scalar field q is conserved. Therefore, there are infinite number of invariants (Smith *et al.* 2002). Following the Kolmogorov-Kraichnan phenomenology of 2D Navier-Stokes turbulence, the two quadratic invariants that determine the cascade directions in generalised 2D turbulence are:

$$E_G = \langle \psi q \rangle, \quad \Omega_G = \langle q^2 \rangle, \quad (2.5)$$

where we refer to E_G as the generalised energy and Ω_G as the generalised enstrophy with units $[E_G] = [L]^{4-\alpha} [T]^{-2}$ and $[\Omega_G] \sim [L]^{4-2\alpha} [T]^{-2}$. The angle brackets $\langle \cdot \rangle$ denote spatiotemporal averaging. Multiplying (2.1) by ψ and integrating over space and time, we can derive the evolution equation of the generalised energy, yielding

$$0 = -\epsilon_+ - \epsilon_- + \epsilon, \quad (2.6)$$

where the left hand side $d_t E_G = 0$ due to statistical stationarity, $\epsilon_+ = -\nu_+ \langle \psi \nabla^{2n} q \rangle$ is the small scale dissipation rate, $\epsilon_- = -\nu_- \langle \psi \nabla^{-2m} q \rangle$ is the large scale dissipation rate and $\epsilon = \langle \psi f_q \rangle$ is the injection rate of the generalised energy. Similarly, if we multiply (2.1) with q and integrate over space and time, the evolution equation of the generalised enstrophy reads as

$$0 = -\xi_+ - \xi_- + \xi, \quad (2.7)$$

where the left hand side $d_t \Omega_G = 0$ due to statistical stationarity, $\xi_+ = -\nu_+ \langle q \nabla^{2n} q \rangle$ is the small scale dissipation rate, $\xi_- = -\nu_- \langle q \nabla^{-2m} q \rangle$ is the large scale dissipation rate and $\xi = \langle q f_q \rangle$ is the injection rate of the generalised enstrophy.

The equivalent expression of (2.2) in Fourier space is

$$\hat{q}(\mathbf{k}, t) = -k^\alpha \hat{\psi}(\mathbf{k}, t) \quad (2.8)$$

where $k = \sqrt{k_x^2 + k_y^2}$ is the isotropic two-dimensional wavenumber. The notation $\hat{\cdot}$ denotes the Fourier transform coefficients. The spectra of the two quadratic invariants can be connected using the relationship (2.8) together with Parseval's theorem to get

$$\Omega_G(k) = k^\alpha E_G(k). \quad (2.9)$$

Now, the spectra of the two quadratic invariants in the inertial range can be derived following Kolmogorov (1941) scaling arguments, where the spectral flux is assumed to be constant in the inertial range and the spectral densities $E_G(k)$ and $\Omega_G(k)$ are only functions of the local scale and spectral flux. Hence, using dimensional arguments for the generalised energy and enstrophy flux we get

$$\frac{k E_G(k)}{\tau_E(k)} = \epsilon = \text{const.}, \quad \tau_E(k) = [k^{5-\alpha} E_G(k)]^{-1/2} \quad (2.10)$$

$$\frac{k \Omega_G(k)}{\tau_\Omega(k)} = \xi = \text{const.}, \quad \tau_\Omega(k) = [k^{5-2\alpha} \Omega_G(k)]^{-1/2} \quad (2.11)$$

where $\tau_E(k)$ is the local timescale that takes E_G to be transferred across wavenumbers. Then, by combining (2.10) and (2.11) with (2.9) we obtain the following power laws that

depend on the value of α

$$E_G(k) \propto \epsilon^{2/3} k^{(\alpha-7)/3}, \quad \Omega_G(k) \propto \epsilon^{2/3} k^{(4\alpha-7)/3}, \quad (2.12)$$

$$E_G(k) \propto \xi^{2/3} k^{(-\alpha-7)/3}, \quad \Omega_G(k) \propto \xi^{2/3} k^{(2\alpha-7)/3}, \quad (2.13)$$

for wavenumbers in the inertial ranges above and below the intermediate forcing wavenumber k_f .

The flux Π is a measure of the nonlinear cascade of a conserved quantity in turbulence (Alexakis & Biferale 2018). The energy flux for a circle of radius k in the 2D wavenumber space is the total energy transferred from the modes within the circle to the modes outside the circle. Consequently, we define the flux of generalised energy $\Pi_E(k, t)$ and enstrophy $\Pi_\Omega(k, t)$ as

$$\Pi_E(k, t) = \sum_{k' \leq k} T_E(k', t), \quad (2.14a)$$

$$\Pi_\Omega(k, t) = \sum_{k' \leq k} T_\Omega(k', t), \quad (2.14b)$$

where $T_E(k, t)$ and $T_\Omega(k, t)$ are the non-linear generalised energy and enstrophy transfers across k

$$T_E(k, t) = \sum_{k \leq |\mathbf{k}| < k + \Delta k} \widehat{\psi}^*(\mathbf{k}, t) \widehat{\mathcal{J}}(\widehat{\psi}, q)(\mathbf{k}, t), \quad (2.15a)$$

$$T_\Omega(k, t) = \sum_{k \leq |\mathbf{k}| < k + \Delta k} \widehat{q}^*(\mathbf{k}, t) \widehat{\mathcal{J}}(\widehat{\psi}, q)(\mathbf{k}, t), \quad (2.15b)$$

where the sum is performed over the Fourier modes with wavenumber amplitude k in a shell of width $\Delta k = 2\pi/L$.

In general we cannot determine the direction of cascade of the two invariants unless there are special relations between the two like Eq. (2.9). A generalised Fjørtoft (1953) argument on the directions of the cascades of two quadratic invariants has been reformulated by Alexakis & Biferale (2022), which essentially states that

$$\text{if } |E_G(k)| \leq ck^{-\alpha} \Omega_G(k) \text{ with } c > 0 \text{ and } \alpha > 0 \text{ then } E_G \text{ cannot cascade forward,} \quad (2.16)$$

and

$$\text{if } \Omega_G(k) \leq ck^\alpha |E_G(k)| \text{ with } c > 0 \text{ and } \alpha > 0 \text{ then } \Omega_G \text{ cannot cascade inversely.} \quad (2.17)$$

In other words, when $\alpha > 0$ then E_G is transferred towards large scales while Ω_G is transferred towards small scales and the opposite is true when $\alpha < 0$. In the next section we demonstrate this rigorously using mathematical inequalities on the injection and dissipation rates of the generalised energy and enstrophy.

3. Bounds

Let us start with Eq. (2.1) and consider the case of small scale dissipation with the power of the Laplace operator $n = 1$ and the large scale diffusion coefficient $\nu_- = 0$. We then have

$$\partial_t q + \mathcal{J}(\psi, q) = \nu_+ \nabla^2 q + f_q, \quad (3.1)$$

where f_q is time independent. The corresponding streamfunction equation can be found using Eq. (2.2), i.e.

$$\partial_t \psi + \mathcal{J}'(\psi, q) = \nu_+ \nabla^2 \psi + f_\psi, \quad (3.2)$$

where $\mathcal{J}'(\psi, q) = -(-\nabla^2)^{-\alpha/2}\mathcal{J}(\psi, q)$. Using the rms velocity $U = \langle |\mathbf{u}|^2 \rangle^{1/2} = \langle |\nabla\psi|^2 \rangle^{1/2}$, we define the dimensionless measures of generalized energy and enstrophy dissipation as:

$$c_\epsilon = \frac{\epsilon_+}{U^3 k_f^{\alpha-1}}, \quad c_\xi = \frac{\xi_+}{U^3 k_f^{2\alpha-1}}. \quad (3.3)$$

The Reynolds number based on the rms velocity field is defined as

$$\text{Re} = \frac{U}{k_f \nu_+}, \quad (3.4)$$

where the forcing wavenumber $k_f = \langle |\nabla^2 f_\psi|^2 \rangle^{1/2} / \langle |f_\psi|^2 \rangle^{1/2}$. Now let us consider separately the cases for positive and negative α .

3.1. Positive α

In statistically stationary state, we have the balance between the dissipation and the injection of generalised enstrophy and so from Eqn. (2.7) we have $\xi_+ = \nu_+ \langle |\nabla q|^2 \rangle = \langle q f_q \rangle$. Using equation (2.8) we can write $\xi_+ = \langle q f_q \rangle \leq k_f^{2\alpha} \langle \psi f_\psi \rangle$ and with the Cauchy-Schwarz inequality we get

$$\xi_+ \leq k_f^{2\alpha-1} \langle |\psi|^2 \rangle^{1/2} \langle |f_\psi|^2 \rangle^{1/2} = k_f^{2\alpha-1} U F_\psi, \quad (3.5)$$

where $F_\psi = \langle |f_\psi|^2 \rangle^{1/2}$ and

$$\langle |\psi|^2 \rangle^{1/2} \leq C k_f^{-1} \langle |\mathbf{u}|^2 \rangle^{1/2} = C k_f^{-1} U, \quad (3.6)$$

using the Poincare inequality as ψ is a lower derivative than the velocity field \mathbf{u} , where C is a constant that depends on the domain geometry. Thus, Eq. (3.5) yields a bound on the generalised enstrophy dissipation rate at the small scales in terms of forcing.

Now we multiply Eq. (3.2) by a smoothly varying doubly differentiable function ϕ ,

$$\phi \partial_t \psi + \phi \mathcal{J}'(\psi, q) = \nu_+ \phi \nabla^2 \psi + \phi f_\psi.$$

Performing a spatio-temporal averaging and changing the order of differentiation during the integration by parts, we get

$$\langle (\mathbf{u} \cdot \nabla \phi) \psi \rangle = \nu_+ \langle \psi \nabla^2 \phi \rangle + \langle \phi f_\psi \rangle. \quad (3.7)$$

For the left hand side term of (3.7), we use the Hölder's and Cauchy-Schwartz inequalities to get

$$\begin{aligned} \langle (\mathbf{u} \cdot \nabla \phi) \psi \rangle &\leq \|\nabla \phi\|_\infty \langle |\psi|^2 \rangle^{1/2} \langle |\mathbf{u}|^2 \rangle^{1/2} \\ &\leq C \|\nabla \phi\|_\infty k_f^{-1} U^2. \end{aligned} \quad (3.8)$$

Similarly for the first term on the right hand side of (3.7), we can write

$$\nu_+ \langle \psi \nabla^2 \phi \rangle \leq \nu_+ \langle |\psi|^2 \rangle^{1/2} \langle |\nabla^2 \phi|^2 \rangle^{1/2}. \quad (3.9)$$

Putting equations (3.8) and (3.9) back in (3.7), we get

$$\langle \phi f_\psi \rangle \leq C \|\nabla \phi\|_\infty k_f^{-1} U^2 + \nu_+ \langle |\psi|^2 \rangle^{1/2} \langle |\nabla^2 \phi|^2 \rangle^{1/2}. \quad (3.10)$$

Now, by letting $\phi = f_\psi / F_\psi$ we can simplify the expression and obtain a bound on the forcing, namely

$$F_\psi \leq C_1 U^2 + C_2 \nu_+ k_f U, \quad (3.11)$$

where C_1, C_2 are constants that depend on the form of the forcing function and the

domain geometry. Substituting (3.11) in the expression for the generalised enstrophy dissipation rate (3.5) we obtain the following bound,

$$\xi_+ \leq k_f^{2\alpha-1} U (C_1 U^2 + C_2 \nu_+ k_f U), \quad (3.12)$$

which in non-dimensional form can be written as,

$$c_\xi \leq C_1 + C_2 Re^{-1}, \quad (3.13)$$

dividing by $k_f^{2\alpha-1} U^3$ and using the definitions (3.3) and (3.4). So, as $Re \rightarrow \infty$ the generalised enstrophy dissipation rate $c_\xi \rightarrow \text{constant}$, which is independent of the viscosity ν_+ and amplitude of the velocity field U . This result is similar to 2D Navier-Stokes turbulence (i.e. $\alpha = 2$), where the enstrophy dissipation rate goes to a constant as $Re \rightarrow \infty$. Thus, for any $\alpha > 0$ we find that a generalised 2D turbulent flow will lead to a constant c_ξ as $Re \rightarrow \infty$.

We then look to bound the generalised energy dissipation rate given by $\epsilon_+ = \nu_+ \langle \psi \nabla^2 q \rangle$. Using the Cauchy-Schwarz inequality, we get

$$\begin{aligned} \epsilon_+ &\leq \nu_+ \langle |\nabla \psi|^2 \rangle^{1/2} \langle |\nabla q|^2 \rangle^{1/2} \\ &\leq \nu_+^{1/2} U \xi_+^{1/2}. \end{aligned} \quad (3.14)$$

Using the bound for ξ_+ from Eq. (3.12), this inequality simplifies to

$$c_\epsilon \leq Re^{-1/2} (C_1 + C_2 Re^{-1})^{1/2}, \quad (3.15)$$

dividing by $U^3 k_f^{\alpha-1}$ and using the definitions (3.3) and (3.4). Thus, $c_\epsilon \rightarrow 0$ as $Re \rightarrow \infty$, implying that there is no forward cascade of generalised energy for $\alpha > 0$ in the limit of infinite Reynolds number.

3.2. Negative α

In a similar fashion to positive α , in statistically stationary state we have the balance between the dissipation and the injection rate of generalised energy. So from Eq. (2.6) we have $\epsilon_+ = \nu_+ \langle \psi \nabla^2 q \rangle = \langle \psi f_q \rangle$. Using the Cauchy-Schwarz and Poincare inequalities we get

$$\begin{aligned} \epsilon_+ &\leq \langle |\psi|^2 \rangle^{1/2} \langle |f_q|^2 \rangle^{1/2} \\ &\leq C k_f^{-1} U F_q, \end{aligned} \quad (3.16)$$

where $F_q = \langle |f_q|^2 \rangle^{1/2}$. Now, we multiply Eq. (3.1) by a smoothly varying doubly differentiable function ϕ ,

$$\phi \partial_t q + \phi \mathcal{J}(\psi, q) = \nu_+ \phi \nabla^2 q + \phi f_q. \quad (3.17)$$

By performing spatiotemporal averaging and changing the order of differentiation during the integration by parts, we get

$$\langle (\mathbf{u} \cdot \nabla \phi) q \rangle = \nu_+ \langle q \nabla^2 \phi \rangle + \langle \phi f_q \rangle \quad (3.18)$$

For the left hand side term of (3.18), we use the Hölder's and Cauchy-Schwartz inequalities to get

$$\begin{aligned} \langle (\mathbf{u} \cdot \nabla \phi) q \rangle &\leq \| \nabla \phi \|_\infty \langle |q|^2 \rangle^{1/2} \langle |\mathbf{u}|^2 \rangle^{1/2} \\ &\leq \tilde{C} \| \nabla \phi \|_\infty k_f^{\alpha-1} U^2, \end{aligned} \quad (3.19)$$

using also the Poincare inequality as q is a lower derivative of the velocity field \mathbf{u} for $\alpha < 0$ and so

$$\langle |q|^2 \rangle^{1/2} \leq \tilde{C} k_f^{\alpha-1} \langle |\mathbf{u}|^2 \rangle^{1/2} = \tilde{C} k_f^{\alpha-1} U, \quad (3.20)$$

where \tilde{C} is a constant that depends on the domain geometry. Similarly for the first term of the right hand side of Eq. (3.18), we can write

$$\begin{aligned} \nu_+ \langle q \nabla^2 \phi \rangle &\leq \nu_+ \langle |q|^2 \rangle^{1/2} \langle |\nabla^2 \phi|^2 \rangle^{1/2} \\ &\leq \tilde{C} \nu_+ k_f^{\alpha-1} U \langle |\nabla^2 \phi|^2 \rangle^{1/2} \end{aligned} \quad (3.21)$$

Putting equations (3.19) and (3.21) back in (3.18), we get

$$\langle \phi f_q \rangle \leq \|\nabla \phi\|_\infty k_f^{\alpha-1} U^2 + \tilde{C} \nu_+ k_f^{\alpha-1} U \langle |\nabla^2 \phi|^2 \rangle^{1/2} \quad (3.22)$$

Now, by letting $\phi = f_q/F_q$ we can simplify the expression and obtain a bound on the forcing, namely

$$F_q \leq k_f^\alpha (C_3 U^2 + C_4 \nu_+ k_f U), \quad (3.23)$$

where C_3, C_4 are constants that depend on the form of the forcing function and the domain geometry. Substituting (3.23) in the expression for the generalised energy dissipation rate (3.16) we obtain the following bound

$$\epsilon_+ \leq k_f^{\alpha-1} U (C_3 U^2 + C_4 \nu_+ k_f U) \quad (3.24)$$

which in non-dimensional form can be written as,

$$c_\epsilon \leq C_3 + C_4 Re^{-1} \quad (3.25)$$

dividing by $k_f^{\alpha-1} U^3$ and using the definitions (3.3) and (3.4). Thus, as $Re \rightarrow \infty$ we find that a generalised 2D turbulent flow will lead to a constant generalised energy dissipation rate c_ϵ , independent of the viscosity ν_+ and amplitude of the velocity field U for any $\alpha < 0$.

We then look to bound the generalised enstrophy dissipation rate $\xi_+ = \nu_+ \langle |\nabla q|^2 \rangle$ which can be written in the spectral space as

$$\xi_+ = \nu_+ \sum_{\mathbf{k}} k^{1+\frac{\alpha}{2}} k^{1-\frac{\alpha}{2}} |\hat{q}(\mathbf{k}, t)|^2. \quad (3.26)$$

Using the Cauchy-Schwarz inequality we get the expression

$$\xi_+ \leq \nu_+ \left(\sum_{\mathbf{k}} k^{2+\alpha} |\hat{q}(\mathbf{k}, t)|^2 \right)^{\frac{1}{2}} \left(\sum_{\mathbf{k}} k^{2-\alpha} |\hat{q}(\mathbf{k}, t)|^2 \right)^{\frac{1}{2}}. \quad (3.27)$$

For the first term in the brackets we can use the Poincare inequality to get

$$\left(\sum_{\mathbf{k}} k^{2+\alpha} |\hat{q}(\mathbf{k}, t)|^2 \right)^{\frac{1}{2}} = \left(\sum_{\mathbf{k}} k^{2+3\alpha} |\hat{\psi}(\mathbf{k}, t)|^2 \right)^{\frac{1}{2}} \leq C_5 k_f^{3\alpha/2} U, \quad (3.28)$$

where C_5 is a constant that depends on the form of the forcing function and the domain geometry. Now, the second term in the brackets can be written as

$$\left(\sum_{\mathbf{k}} k^{2-\alpha} |\hat{q}(\mathbf{k}, t)|^2 \right)^{\frac{1}{2}} = \langle q \nabla^2 \psi \rangle^{1/2} = (\epsilon_+ / \nu_+)^{1/2}. \quad (3.29)$$

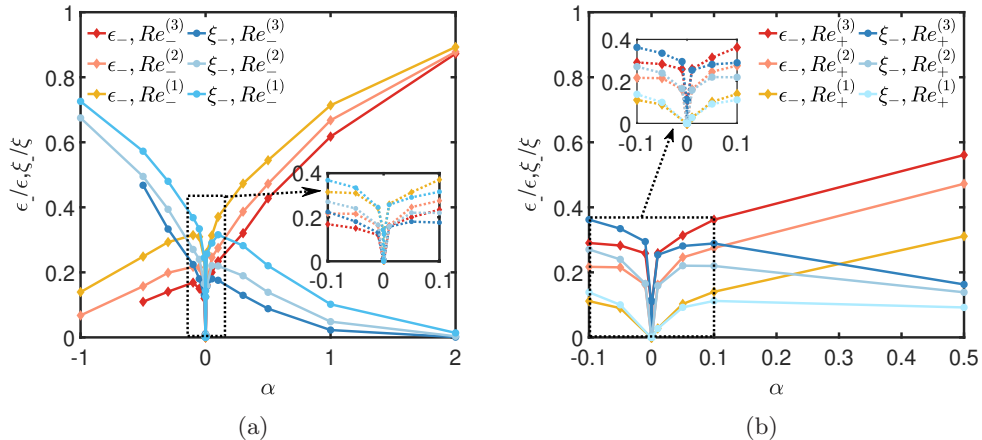


Figure 1: Normalised large scale dissipation rate of generalised energy ϵ_-/ϵ and enstrophy ξ_-/ξ as a function of α . Plot a) shows the bifurcation diagram for fixed $Re_+ = 1381$ and increasing values of Re_- , where $Re_-^{(1)} = 10^6$, $Re_-^{(2)} = 4 \times 10^7$ and $Re_-^{(3)} = 2 \times 10^9$. Plot b) shows the bifurcation diagram for fixed $Re_- = 4 \times 10^7$ and increasing value of Re_+ , where $Re_+^{(1)} = 345$, $Re_+^{(2)} = 1381$ and $Re_+^{(3)} = 3450$.

Putting equations (3.28) and (3.29) back in (3.27), we get

$$\xi_+ \leq C_5 \nu_+^{1/2} k_f^{3\alpha/2} U \epsilon_+^{1/2}. \quad (3.30)$$

Using the bound for ϵ_+ from Eq. (3.24), this inequality simplifies to

$$c_\xi \leq Re^{-1/2} (C_1 + C_2 Re^{-1})^{1/2} \quad (3.31)$$

dividing by $U^3 k_f^{2\alpha-1}$ and using the definitions (3.3) and (3.4). Thus, $c_\xi \rightarrow 0$ as $Re \rightarrow \infty$, implying that there is no forward cascade of generalised enstrophy for $\alpha < 0$ in the limit of infinite Reynolds number.

In summary, the bounds we derived for positive and negative α demonstrate the transition of the cascades between the generalised energy and enstrophy. In other words, for $\alpha > 0$ the bounds suggest that in the limit of infinite Reynolds number ϵ_+ tends to zero due to the inverse cascade, and ξ_+ remains finite due to the dissipation anomaly of the forward cascade, while the opposite is true for $\alpha < 0$.

4. Numerical Results

4.1. Transition of generalised energy and enstrophy cascades

To investigate the transition of the cascades, we numerically simulate the generalised vorticity equations (2.1)-(2.2) in the limit of large Reynolds numbers by varying α systematically. The details of the numerical method and simulation parameters used are mentioned in Appendix A. We quantify the variation in the generalised energy and enstrophy fluxes to large scales using the large scale dissipation rates ϵ_- and ξ_- defined in Eqs. (2.6), (2.7). For the parameters explored, ϵ_- and ξ_- are localised at large length scales giving an estimate of the flux to large scales occurring through an inverse cascade or transfer.

In Fig. 1 we show the large scale dissipation rates normalised by their respective injection rates, ϵ_-/ϵ and ξ_-/ξ , as a function of α . In Fig. 1a we consider different values

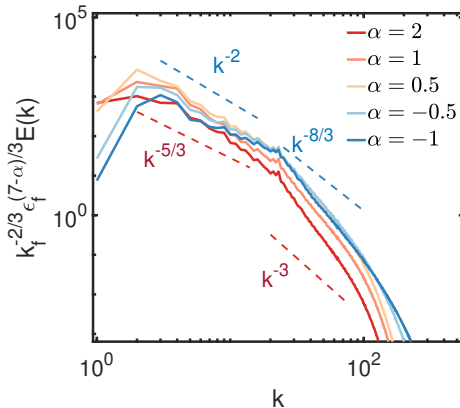


Figure 2: Energy spectra for different α along with their theoretical exponents in red ($\alpha = 2$) and blue ($\alpha = -1$) are shown. The spectra are obtained from DNS with $Re_+ = 1381$, $Re_- = 4 \times 10^7$ and $k_f = 16\sqrt{2}$.

of Re_- with fixed Re_+ , while in Fig. 1b we consider different values of Re_+ with fixed Re_- . We find that for $\alpha = 2$ the energy dissipation is predominantly at large length scales due to the inverse cascade of energy in 2D Navier-Stokes turbulence. On the other hand, for $\alpha = -1$ we observe the transition of the cascades with the energy to be predominantly dissipated at small scales suggesting a forward cascade of energy. For intermediate values of α we find that energy is dissipated at both large and small scales implying the presence of a dual cascade.

As seen from Fig. 1a, for a given Re_+ increasing Re_- leads to smaller inverse cascade of both the generalised energy and enstrophy. In Figure 1b for a fixed Re_- increasing Re_+ leads to smaller forward cascade of both the generalised energy and enstrophy. Thus, we find that the behaviour close to $\alpha = 0$ depends strongly on the control parameters Re_+ and Re_- as the nonlinearity, which leads to the cascade, vanishes as $\alpha \rightarrow 0$. At $\alpha = 0$ there is no cascade as the nonlinearity vanishes, i.e. $\mathcal{J}(\psi, \psi) = 0$ by definition. This leads both the forcing and dissipation to be localised at the wavenumber k_f . We refer to $\alpha = 0$ as the threshold where the cascades vanish for any value of the dissipation coefficients. For the simulation parameters that are explored here, the small scale dissipation dominates over the large scale dissipation near $\alpha \approx 0$ implying that the dissipation due to large scale friction is negligible, namely $\epsilon_- \ll 1$. The exact behaviour close to $\alpha = 0$ will be discussed in section 4.2.

In Fig. 2 we show the generalised energy spectrum for different values of α . The dashed lines show the phenomenological predictions from Eqs. (2.12), (2.13). The red dashed lines show the prediction for $\alpha = 2$ and the blue dashed lines show the prediction for $\alpha = -1$. We see that the generalised energy spectra in the range $k_{min} < k < k_f$ have exponents close to the predictions (2.12), while in the range $k_f < k < k_{max}$ the exponents are far from the phenomenological predictions. This is also seen in 2D Navier-Stokes turbulence with $\alpha = 2$, where the exponent of the range $k_f < k < k_{max}$ depends on the small scale Reynolds number (Boffetta & Ecke 2012). Simulations at very high resolutions are required to shed light on the differences in the spectral exponents for the different values of α and the validity of Kolmogorov type arguments to determine the exponents.

Figure 3 shows the fluxes of generalised energy and enstrophy, normalized with their respective injection rates, for different values of α . For the Navier-Stokes model ($\alpha = 2$) we

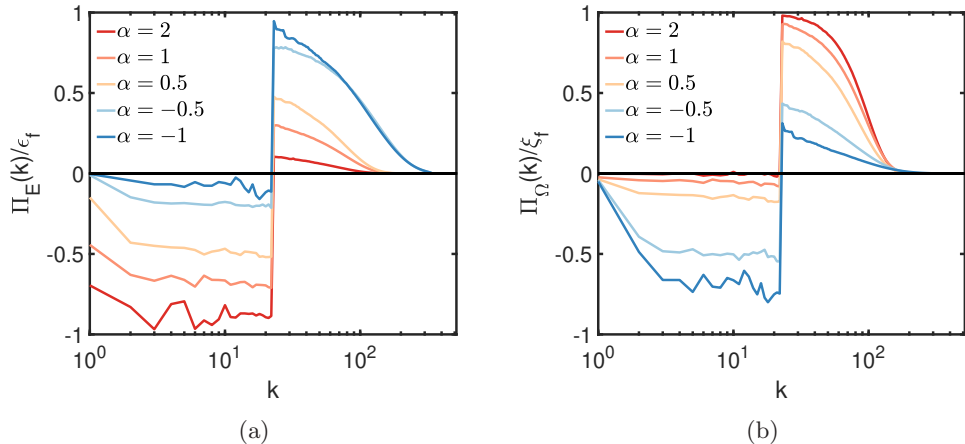


Figure 3: a) Normalized energy flux and b) normalised enstrophy flux for different α . The fluxes are obtained from DNS with $Re_+ = 1381$, $Re_- = 4 \times 10^7$ and $k_f = 16\sqrt{2}$.

see that the energy cascades mostly to large scales (or low k) while the enstrophy cascades mostly to small scales (or high k). For the $\alpha = -1$ we find the opposite scenario where the energy mostly cascades to small scales while the generalised enstrophy cascades to large scales. Intermediate values of α shows dual cascade where the generalised energy and enstrophy cascade to both large and small scales. This is similar to the cascade transitions seen in other turbulent systems such as in Celani *et al.* (2010), Seshasayanan *et al.* (2014b), Benavides & Alexakis (2017). Close to $\alpha = 0$ we find that the cascade vanishes with energy injection and dissipation occurring at the same length scale.

The top row of Fig. 4 shows the generalised vorticity distribution for different values of α . For $\alpha = 2$, we get the two-dimensional large scale vortices which are generated by the inverse cascade of energy. As α is reduced we see that the vortices become diffused with the sizes of the vortices becoming large. For $\alpha = 1$, Carton *et al.* (2016) found that the distance of vortex merging was generally smaller than for $\alpha = 2$. It was explained that for a point vortex of the form $q(r) = \delta(r)$, the velocity field decreases like $1/r^2$ for the case SQG model ($\alpha = 1$) while for the standard Navier-Stokes model ($\alpha = 2$) the velocity reduces like $1/r$ from the core of the vortices. Hence, the region of influence of the vortices decreases as we reduce α . To distinguish the behaviour of the classical vorticity from the generalised vorticity, we show in the bottom row of Fig. 4 the contour plot of the classical vorticity defined as $\omega = \nabla^2\psi$ for all values of α . As seen from the figures the classical vorticity goes to smaller length scales as α is reduced. For $\alpha < 0$ we observe a few vortices along with many filamentary structures that resemble the thin vortex filaments observed in 3D homogeneous isotropic turbulence.

4.2. Near the threshold $\alpha = 0$

We investigate the behaviour of the system close to the threshold $\alpha = 0$. At $\alpha = 0$ the nonlinearity vanishes and the flow becomes laminar. As one moves away from the threshold, the flow remains laminar until it undergoes a linear instability. Here the instability is found to occur at smaller length scales than the laminar flow, unlike the negative viscosity instability that is observed in many 2D flows. The threshold of the instability is found to be the same for both positive and negative values of α . For simplicity we report on the critical point of the instability α_c as we increase α away

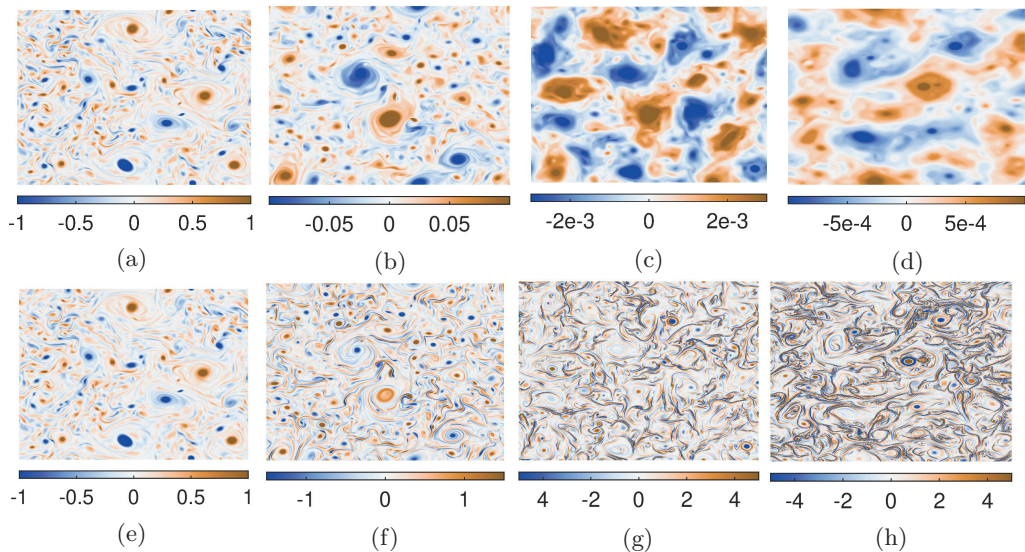


Figure 4: Generalised vorticity field for a) $\alpha = 2.0$ b) $\alpha = 1.0$ c) $\alpha = -0.5$ d) $\alpha = -1.0$. The corresponding classical vorticity fields are shown in e) $\alpha = 2.0$ f) $\alpha = 1.0$ g) $\alpha = -0.5$ and h) $\alpha = -1.0$. For $\alpha = 2, 1$ and -0.5 the colorbar has been capped at 50% of the maximum value and at 10% for $\alpha = -1$ to emphasise the structures of the fields. The fields are obtained from DNS with $Re_+ = 1381$, $Re_- = 4 \times 10^7$ and $k_f = 16\sqrt{2}$.

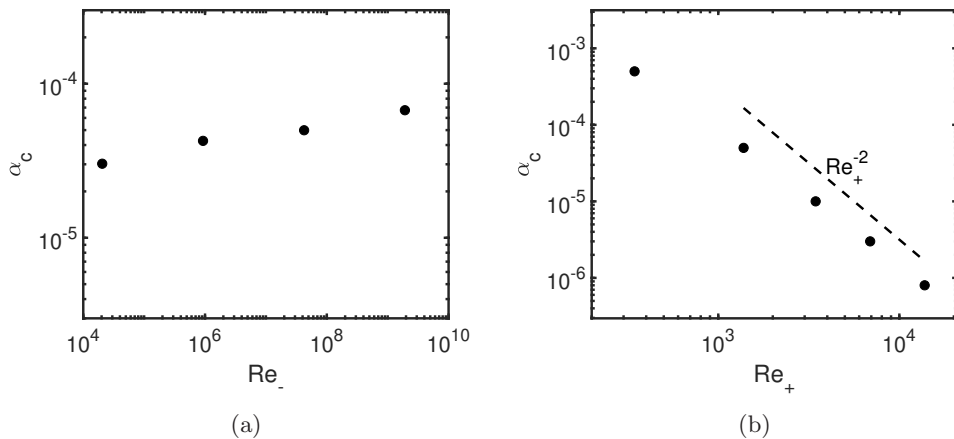


Figure 5: Figure shows the variation of α_c as a function of a) Re_- and b) Re_+ . The dashed line in figure b) denotes the scaling $\alpha_c \propto Re_+^{-2}$.

from zero to positive values. In Fig. 5 we show the critical point of the instability α_c as a function of Re_- and Re_+ . For the parameters of $Re_+ = 1381$, $Re_- = 4 \times 10^7$ at $\alpha = 0$ the large scale friction is negligible, thus we find that the instability threshold α_c is almost independent of Re_- (see Fig. 5a). We also find that the threshold decreases like a power law as Re_+ increases (see Fig. 5b), thus neglecting the effect of large scale friction we expect that $\alpha_c \rightarrow 0$ as $Re_+ \rightarrow \infty$. The dependence on Re_+ indicates that the behaviour very close to the critical point is sensitive to the dissipation coefficients.

The scaling of α_c with Re_+ can be found by doing a perturbation around $\alpha = 0$. We write the fields as a sum of the base flow and a perturbation, $q = q_b + \tilde{q}$, $\psi = \psi_b + \tilde{\psi}$, where the terms with the subscript b denote the base flow component and the terms with $\tilde{}$ denote the perturbation fields. Substituting this decomposition into the nonlinear term of equation (2.1) we get, $\mathcal{J}(\psi, q) = \mathcal{J}(\psi_b, q_b) + \mathcal{J}(\tilde{\psi}, q_b) + \mathcal{J}(\psi_b, \tilde{q}) + \mathcal{J}(\tilde{\psi}, \tilde{q})$. The term $\mathcal{J}(\psi_b, q_b)$ is zero for the laminar solution and the term $\mathcal{J}(\tilde{\psi}, \tilde{q})$ can be neglected as we are looking at the linear onset of the instability. Thus we get,

$$\mathcal{J}(\psi, q) \approx \mathcal{J}(\tilde{\psi}, q_b) + \mathcal{J}(\psi_b, \tilde{q}). \quad (4.1)$$

We express the terms in the Fourier space using the relation (2.8) and then expand the above expression in powers of α . In the limit of $\alpha \rightarrow 0$ we can expand $k^\alpha = k_f^\alpha (1 + \alpha \log(\frac{k}{k_f}) + O(\alpha^2))$. Then, equation (4.1) at leading order in α will take the form

$$\mathcal{J}(\psi, q) \approx \alpha \left[\mathcal{J}(\tilde{\psi}, \phi_b) + \mathcal{J}(\psi_b, \tilde{\phi}) \right] + O(\alpha^2), \quad (4.2)$$

where the Fourier coefficients of the fields ϕ_b and $\tilde{\phi}$ are defined as

$$\phi_b(\mathbf{k}, t) = -k_f^\alpha \log\left(\frac{k}{k_f}\right) \psi_b(\mathbf{k}, t), \quad \tilde{\phi}(\mathbf{k}, t) = -k_f^\alpha \log\left(\frac{k}{k_f}\right) \psi(\mathbf{k}, t). \quad (4.3)$$

Using Eq. (4.2) we can derive a scaling of α_c with Re_+ from the balance between the non-linear term $J(\psi, q)$ and the dissipation term $\nu_+ \nabla^{2n} \tilde{\psi}$ where $n = 2$. At the threshold α_c of the linear instability we use Eqs. (4.2) and (4.3) to find the following leading order scaling

$$J(\psi, q) \sim \alpha_c \frac{f_0}{\nu_+ k_f^2} g_1 \left(\frac{k_i}{k_f}\right) \tilde{\psi}, \quad (4.4)$$

$$\nu_+ \nabla^4 \tilde{\psi} \sim \nu_+ k_f^4 g_2 \left(\frac{k_i}{k_f}\right) \tilde{\psi}, \quad (4.5)$$

where k_i denotes the typical wavenumber of the unstable mode $\tilde{\psi}$ and g_1, g_2 are two functions of k_i/k_f . Equating (4.4) with (4.5) we get,

$$\alpha_c \frac{f_0}{\nu_+ k_f^2} \sim \nu_+ k_f^4 g_3 \left(\frac{k_i}{k_f}\right), \quad (4.6)$$

where g_3 is a function of k_i/k_f . We find that the ratio k_i/k_f remains almost constant as we vary Re_+ over a few decades, which leads to the following scaling law for the threshold of the instability

$$\alpha_c \sim Re_+^{-2}. \quad (4.7)$$

This scaling law is denoted by the dashed line in Fig. 5b and has a good agreement with the thresholds found numerically for different Re_+ .

4.3. Locality of cascades - α dependence

We quantify the locality of the nonlinear triadic interactions by analysing the transfer rate of generalised energy transferred via the generalised vorticity advection term from one shell of wavenumbers $Q < k < Q + \Delta k$ to another shell of wavenumbers $K < k < K + \Delta k$. We define this shell to shell transfer function as

$$T_E(K, Q, t) = \langle \psi_K(\mathbf{u} \cdot \nabla q_Q) \rangle, \quad (4.8)$$

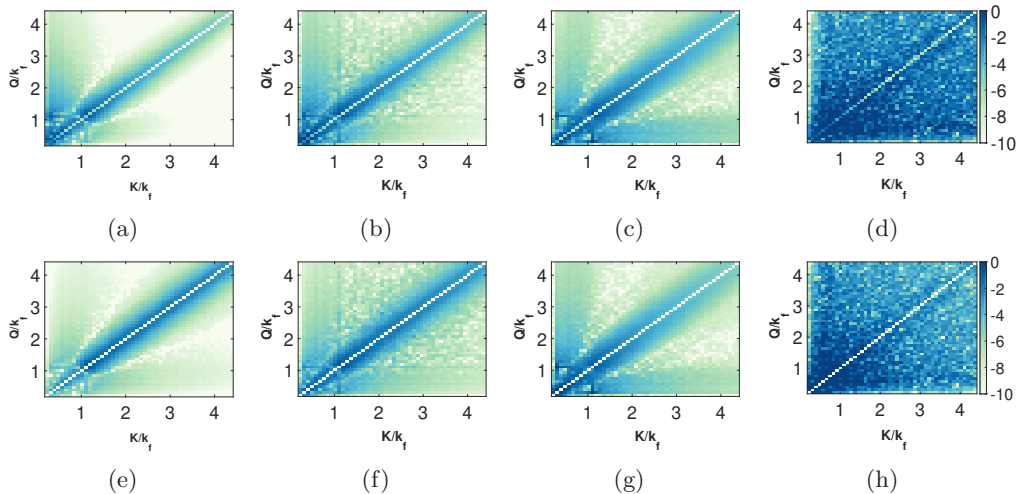


Figure 6: The top row shows shell-to-shell transfers of generalised energy as $\log(|T_E(K, Q)/\epsilon|)$ for (a) $\alpha = 2.0$, (b) $\alpha = 1.0$, (c) $\alpha = -0.5$, and (d) $\alpha = -1.0$. The bottom row shows shell-to-shell transfers of generalised enstrophy as $\log(|T_\Omega(K, Q)/\xi|)$ for (e) $\alpha = 2.0$, (f) $\alpha = 1.0$, (g) $\alpha = -0.5$, and (h) $\alpha = -1.0$. The colorbars are the same for all the plots and are shown only in plots (d) and (h) for clarity. The shell-to-shell transfers are obtained from DNS with $Re_+ = 1381$, $Re_- = 10^6$ and $k_f = 8\sqrt{2}$.

where ψ_K and q_Q are the streamfunction and generalised vorticity field filtered such that only the wavenumbers at shell K and Q are kept, respectively. The transfer term $T_E(K, Q, t)$ conserves the generalised energy, i.e. it does not generate or destroy E_G but it is responsible for the redistribution of the generalised energy across different scales. This is expressed by the fact that $T_E(K, Q, t)$ is antisymmetric under the exchange of K and Q , i.e. $T_E(K, Q, t) = -T_E(Q, K, t)$. Similarly, this is true for the transfer rate of generalised enstrophy from the mode K into the mode Q , which is defined as

$$T_\Omega(K, Q, t) = \langle q_K(\mathbf{u} \cdot \nabla q_Q) \rangle. \quad (4.9)$$

The contour plots in the top row of Fig. 6 show in logarithmic scale the absolute value of the time averaged shell to shell transfer function $T_E(K, Q)$ normalised by the energy injection rate ϵ for a) $\alpha = 2.0$ b) $\alpha = 1.0$, c) $\alpha = -0.5$ and d) $\alpha = -1.0$. For $\alpha = 2$ the shell to shell transfer $T_E(K, Q)$ is mostly concentrated at $K/k_f < 1$, $Q/k_f < 1$ and close to the diagonal $K = Q$, indicating that generalised energy cascades to large scales and mostly via local interactions. For values of $\alpha < 2$, we observe that the transfer becomes more significant at $K/k_f > 1$ and $Q/k_f > 1$ and this is because the cascade transitions more and more to small scales. Moreover, for $\alpha = 1$ and -0.5 the shell to shell transfer $T_E(K, Q)$ happens not only locally close to $K = Q$ but there are also two non-local branches, which become more and more significant as $\alpha \rightarrow -0.5$. These are the vertical branch, which is at the wavenumber range $K/k_f < 1$ along the wavenumbers Q/k_f and the horizontal branch, which is at the wavenumber range $Q/k_f < 1$ along the wavenumbers K/k_f . At $\alpha = -1$, we find that $T_E(K, Q)$ is fully non-local spanning the whole range of wavenumbers.

In a similar fashion the contour plots in the bottom row of Fig. 6 show in logarithmic scale the absolute value of the time averaged shell to shell transfer function $T_\Omega(K, Q)$ normalised by the energy injection rate ξ for e) $\alpha = 2.0$ f) $\alpha = 1.0$, g) $\alpha = -0.5$ and

h) $\alpha = -1.0$. For $\alpha = 2$ the shell to shell transfer $T_\Omega(K, Q)$ occurs predominantly at $K/k_f > 1$, $Q/k_f > 1$ and close to the diagonal $K = Q$, indicating that generalised enstrophy cascades to small scales though local interactions in wavenumber. For values of $\alpha < 2$, we observe that $T_\Omega(K, Q)$ turns gradually to low wavenumber, i.e. at $K/k_f < 1$ and $Q/k_f < 1$ and this happens since the cascade transitions to large scales. In addition, for $\alpha = 1$ and -0.5 the shell to shell transfer happens via three branches. One local branch at $K = Q$ and two non-local branches, which become more and more significant as $\alpha \rightarrow -0.5$. Again these branches are the vertical and horizontal branches that have similar pattern to the non-local branches of $T_E(K, Q)$. Finally, at $\alpha = -1$, we also find that $T_\Omega(K, Q)$ is fully non-local with a wide spread across the wavenumbers.

The fact that the cascades of the generalised energy and enstrophy become gradually non-local as we go from positive to negative values of α is a notion clearly at variance with the typical locality assumption of the Kolmogorov phenomenology. This might be a reason why the energy spectra in Fig. 2 do not agree with the scaling predictions from Eqs. (2.12) and (2.13), which are drawn in the plot for comparison.

5. Conclusion

In this paper we focus on the theoretical and numerical analysis of the cascades in generalised 2D turbulence by systematically varying the parameter α of the model. The value and sign of α determines if the cascade would be inverse, forward or bidirectional. This suggests that there is some critical α_c at which a transition happens in the direction of the cascades. At the threshold $\alpha = 0$ the nonlinear term vanishes and the flow is laminar. We find that as we move away from $\alpha = 0$ the laminar flow undergoes a linear small wavelength instability at a critical value α_c which is the same both for positive and negative α . We observe that $\alpha_c \approx \text{const.}$ as we increase Re_- , however $\alpha \propto Re_+^{-2}$ as Re_+ increases. This scaling is also verified theoretically by doing a perturbation analysis.

For $\alpha > 0$ using mathematical inequalities we are able to bound the dimensionless dissipation rates of generalised energy $c_\epsilon \equiv \epsilon/(U^3 k_f^{\alpha-1}) \leq Re^{-1/2}(C_1 + C_2 Re^{-1})^{1/2}$ and enstrophy $c_\xi \equiv \xi/(U^3 k_f^{2\alpha-1}) \leq C_1 + C_2 Re^{-1}$. These bounds state that as $Re \rightarrow \infty$ then c_ϵ tends to zero due to the inverse cascade, while c_ξ remains finite due to the dissipation anomaly of the forward cascade. On the other hand, for $\alpha < 0$ we obtain the bounds $c_\epsilon \leq C_1 + C_2 Re^{-1}$ and $c_\xi \leq Re^{-1/2}(C_1 + C_2 Re^{-1})^{1/2}$. This behaviour is due to the transition of the cascades, where c_ϵ remains finite due to the dissipation anomaly of the forward cascade, while c_ξ tends to zero due to the inverse cascade.

By varying α in numerical simulations we confirm this picture; meaning that when $\alpha > 0$ then generalised energy E_G cascades inversely while generalised enstrophy Ω_G cascades forward and the opposite happens when $\alpha < 0$ (see Fig. 1). Moreover, we find that the amount of dissipation rates of E_G and Ω_G depend on the system parameters Re_- and Re_+ . This transition from positive to negative alpha is also clear from the spectral fluxes (see Fig. 3), which determine the spectral exponents of the energy spectra. The energy spectra at large scales, i.e. at length scales larger than the forcing length scale, seem to agree with Kolmogorov type scalings of the generalised 2D turbulence, however, this is not true for length scales smaller than the forcing length scale. A reason of this discrepancy might be that higher resolution computations are required to shed light on the nonlocal transfers of generalised energy and enstrophy might be the cause of this disagreement. Finally, it is interesting to mention that due to the forward cascade of E_G for $\alpha < 0$ the classical vorticity field, which is dominated by vortex filaments, is reminiscent of the filaments observed in 3D Navier-Stokes turbulence.

	a) $Re_+ = 1381$			b) $Re_- = 4 \times 10^7$			
	$Re_-^{(1)} = 10^6$	$Re_-^{(2)} = 4 \times 10^7$	$Re_-^{(3)} = 2 \times 10^9$	$Re_+^{(1)} = 345$	$Re_+^{(2)} = 1381$	$Re_+^{(3)} = 3450$	$Re_+^{(4)} = 6900$
N	512	1024	2048	1024	1024	1024	1024
k_f	$8\sqrt{2}$	$16\sqrt{2}$	$32\sqrt{2}$	$16\sqrt{2}$	$16\sqrt{2}$	$16\sqrt{2}$	$16\sqrt{2}$

Table 1: Numerical parameters for the two set of runs corresponding to a) fixed Re_+ with varying Re_- and b) fixed Re_- with varying Re_+ .

This study shows that the generalised model of 2D turbulence is another nice setup to study the transition of turbulent cascades. However, this model is unique as this is the first system that shows features that appear in 3D turbulence, like the vortex filaments, emerging in two dimensions. So, further numerical studies are required to understand deeper and relate the dynamics of the vortex filaments in two dimensions to the dissipation anomaly that is present for negative values of α . Further mathematical analysis of this model dissipation anomaly for negative values of α might provide new insights to the regularity of solutions of the 3D Navier-Stokes equations. The study of locality of cascades using the shell to shell transfers from observational and experimental data of geophysical relevance would complement our findings, e.g. for the SQG ($\alpha = 1$) model, and it gives a warning to the community that we should be thinking beyond the Kolmogorov type of arguments.

Appendix A. Numerical Setup

We perform direct numerical simulations (DNSs) in a periodic square domain by numerically integrating using the pseudospectral method (Gottlieb & Orszag 1977). We decompose the streamfunction $\psi(x, y, t)$ into basis functions of Fourier modes, viz.

$$\psi(\mathbf{x}, t) = \sum_{\mathbf{k}=-N/2}^{N/2} \hat{\psi}_{\mathbf{k}}(t) e^{i\mathbf{k} \cdot \mathbf{x}}, \quad (\text{A } 1)$$

where $\hat{\psi}_{\mathbf{k}}$ is the amplitude of the $\mathbf{k} = (k_x, k_y)$ mode of ψ , and N denotes the number of aliased modes in the x and y directions. A third-order Runge-Kutta scheme is used for time advancement. The aliasing errors are removed with the 2/3 rule, which implies that the maximum wavenumber $k_{max} = N/3$. The computations were performed on graphics cards (GPUs), which provided three times speedup in contrast to computations on processors (CPUs). Time-averaged quantities are computed once the system has reached a statistically stationary regime. The numerical parameters we considered are listed in Table 1.

REFERENCES

- ALEXAKIS, A. 2011 Two-dimensional behavior of three-dimensional magnetohydrodynamic flow with a strong guiding field. *Physical Review E* **84** (5), 056330.
- ALEXAKIS, A. & BIFERALE, L. 2018 Cascades and transitions in turbulent flows. *Physics Reports* **767-769**, 1–101.
- ALEXAKIS, A. & BIFERALE, L. 2022 λ -navier–stokes turbulence. *Philosophical Transactions of the Royal Society A: Mathematical, Physical and Engineering Sciences* **380** (2219), 20210243.

- ARBIC, BRIAN K, POLZIN, KURT L, SCOTT, ROBERT B, RICHMAN, JAMES G & SHRIVER, JAY F 2013 On eddy viscosity, energy cascades, and the horizontal resolution of gridded satellite altimeter products. *Journal of Physical Oceanography* **43** (2), 283–300.
- BALWADA, DHUV, LACASCE, JOSEPH H & SPEER, KEVIN G 2016 Scale-dependent distribution of kinetic energy from surface drifters in the gulf of mexico. *Geophysical Research Letters* **43** (20), 10–856.
- BENAVIDES, SANTIAGO JOSE & ALEXAKIS, ALEXANDROS 2017 Critical transitions in thin layer turbulence. *Journal of Fluid Mechanics* **822**, 364–385.
- BOFFETTA, GUIDO & ECKE, ROBERT E 2012 Two-dimensional turbulence. *Annual review of fluid mechanics* **44**, 427–451.
- BURGESS, BH & SHEPHERD, TG 2013 Spectral non-locality, absolute equilibria and kraichnan–leith–batchelor phenomenology in two-dimensional turbulent energy cascades. *Journal of Fluid Mechanics* **725**, 332–371.
- BYRNE, DAVID & ZHANG, JUN A 2013 Height-dependent transition from 3-d to 2-d turbulence in the hurricane boundary layer. *Geophysical research letters* **40** (7), 1439–1442.
- CAMPAGNE, ANTOINE, GALLET, BASILE, MOISY, FRÉDÉRIC & CORTET, PIERRE-PHILIPPE 2014 Direct and inverse energy cascades in a forced rotating turbulence experiment. *Physics of Fluids* **26** (12).
- CARTON, XAVIER, CIANI, DANIELE, VERRON, JACQUES, REINAUD, J & SOKOLOVSKIY, MIKHAIL 2016 Vortex merger in surface quasi-geostrophy. *Geophysical & Astrophysical Fluid Dynamics* **110** (1), 1–22.
- CELANI, ANTONIO, MUSACCHIO, STEFANO & VINCENZI, DARIO 2010 Turbulence in more than two and less than three dimensions. *Physical review letters* **104** (18), 184506.
- CHERTKOV, M., CONNAUGHTON, C., KOLOKOLOV, I. & LEBEDEV, V. 2007 Dynamics of energy condensation in two-dimensional turbulence. *Phys. Rev. Lett.* **99**, 084501.
- DEUSEBIO, ENRICO, BOFFETTA, GUIDO, LINDBORG, ERIK & MUSACCHIO, STEFANO 2014 Dimensional transition in rotating turbulence. *Physical Review E* **90** (2), 023005.
- ECKE, ROBERT E 2017 From 2d to 3d in fluid turbulence: unexpected critical transitions. *Journal of Fluid Mechanics* **828**, 1–4.
- FJØRTOFT, RAGNAR 1953 On the changes in the spectral distribution of kinetic energy for twodimensional, nondivergent flow. *Tellus* **5** (3), 225–230.
- FOUSSARD, ALEXIS, BERTI, STEFANO, PERROT, XAVIER & LAPEYRE, GUILLAUME 2017 Relative dispersion in generalized two-dimensional turbulence. *Journal of Fluid Mechanics* **821**, 358–383.
- FRISCH, URIEL, LESIEUR, MARCEL & SULEM, PIERRE LOUIS 1976 Crossover dimensions for fully developed turbulence. *Physical Review Letters* **37** (14), 895.
- GOTTLIEB, DAVID & ORSZAG, STEVEN A 1977 *Numerical analysis of spectral methods: theory and applications*. SIAM.
- HELD, ISAAC M, PIERREHUMBERT, RAYMOND T, GARNER, STEPHEN T & SWANSON, KYLE L 1995 Surface quasi-geostrophic dynamics. *Journal of Fluid Mechanics* **282**, 1–20.
- IWAYAMA, T., MURAKAMI, S. & WATANABE, T. 2015 Anomalous eddy viscosity for two-dimensional turbulence. *Physics of Fluids* **27**.
- KHATRI, HEMANT, SUKHATME, JAI, KUMAR, ABHISHEK & VERMA, MAHENDRA K 2018 Surface ocean enstrophy, kinetic energy fluxes, and spectra from satellite altimetry. *Journal of Geophysical Research: Oceans* **123** (5), 3875–3892.
- KING, GREGORY P, VOGELZANG, JUR & STOFFELEN, AD 2015 Upscale and downscale energy transfer over the tropical p acific revealed by scatterometer winds. *Journal of Geophysical Research: Oceans* **120** (1), 346–361.
- KOLMOGOROV, ANDREY NIKOLAEVICH 1941 The local structure of turbulence in incompressible viscous fluid for very large reynolds. *Numbers. In Dokl. Akad. Nauk SSSR* **30**, 301.
- KRAICHNAN, ROBERT H 1971 Inertial-range transfer in two-and three-dimensional turbulence. *Journal of Fluid Mechanics* **47** (3), 525–535.
- KRAICHNAN, ROBERT H 1976 Eddy viscosity in two and three dimensions. *Journal of Atmospheric Sciences* **33** (8), 1521–1536.
- LAPEYRE, GUILLAUME 2017 Surface quasi-geostrophy. *Fluids* **2**.
- LARICHEV, VITALY D. & MCWILLIAMS, JAMES C. 1991 Weakly decaying turbulence in an equivalent-barotropic fluid. *Physics of Fluids A* **3**, 938–950.

- LESUR, GEOFFROY & LONGARETTI, P-Y 2011 Non-linear energy transfers in accretion discs mri turbulence-i. net vertical field case. *Astronomy & Astrophysics* **528**, A17.
- LILLY, DOUGLAS K 1969 Numerical simulation of two-dimensional turbulence. *The Physics of Fluids* **12** (12), II-240.
- MARINO, RAFFAELE, MININNI, PABLO DANIEL, ROSENBERG, DUANE & POUQUET, ANNICK 2013 Inverse cascades in rotating stratified turbulence: fast growth of large scales. *Europhysics letters* **102** (4), 44006.
- NASTROM, GD, GAGE, KS & JASPERSON, WH 1984 Kinetic energy spectrum of large-and mesoscale atmospheric processes. *Nature* **310** (5972), 36–38.
- PIERREHUMBERT, RAYMOND T, HELD, ISAAC M & SWANSON, KYLE L 1994a Spectra of local and nonlocal two-dimensional turbulence. *Chaos, Solitons & Fractals* **4** (6), 1111–1116.
- PIERREHUMBERT, RAYMOND T, HELD, ISAAC M & SWANSON, KYLE L 1994b Spectra of local and nonlocal two-dimensional turbulence. *Solitons and Fractals* **4**, 1111–1116.
- READ, PETER L 2001 Transition to geostrophic turbulence in the laboratory, and as a paradigm in atmospheres and oceans. *Surveys in geophysics* **22**, 265–317.
- RHINES, PETER B 1979 Geostrophic turbulence. *Annual Review of Fluid Mechanics* **11** (1), 401–441.
- SCOTT, ROBERT B & WANG, FANGMING 2005 Direct evidence of an oceanic inverse kinetic energy cascade from satellite altimetry. *Journal of Physical Oceanography* **35** (9), 1650–1666.
- SEN, AMRIK, MININNI, PABLO D, ROSENBERG, DUANE & POUQUET, ANNICK 2012 Anisotropy and nonuniversality in scaling laws of the large-scale energy spectrum in rotating turbulence. *Physical Review E* **86** (3), 036319.
- SESHASAYANAN, KANNABIRAN, BENAVIDES, SANTIAGO JOSE & ALEXAKIS, ALEXANDROS 2014a On the edge of an inverse cascade. *Physical Review E* **90** (5), 051003.
- SESHASAYANAN, KANNABIRAN, BENAVIDES, SANTIAGO JOSE & ALEXAKIS, ALEXANDROS 2014b On the edge of an inverse cascade. *Physical Review E - Statistical, Nonlinear, and Soft Matter Physics* **90**.
- SHAO, XIN, ZHANG, NING & TANG, JIE 2023 A physical model for the observed inverse energy cascade in typhoon boundary layers. *Geophysical Research Letters* **50** (18), e2023GL105546.
- SHATS, MICHAEL, BYRNE, DAVID & XIA, HUA 2010 Turbulence decay rate as a measure of flow dimensionality. *Physical review letters* **105** (26), 264501.
- SIEGELMAN, LIA, KLEIN, PATRICE, INGERSOLL, ANDREW P, EWALD, SHAWN P, YOUNG, WILLIAM R, BRACCO, ANNALISA, MURA, ALESSANDRO, ADRIANI, ALBERTO, GRASSI, DAVIDE, PLAINAKI, CHRISTINA & OTHERS 2022 Moist convection drives an upscale energy transfer at jovian high latitudes. *Nature Physics* **18** (3), 357–361.
- SMITH, K. S., BOCCALETTI, G., HENNING, C. C., MARINOV, I., TAM, C. Y., HELD, I. M. & VALLIS, G. K. 2002 Turbulent diffusion in the geostrophic inverse cascade. *Journal of Fluid Mechanics* **469**, 13–48.
- SMITH, LESLIE M, CHASNOV, JEFFREY R & WALEFFE, FABIAN 1996 Crossover from two-to three-dimensional turbulence. *Physical review letters* **77** (12), 2467.
- SOZZA, ALESSANDRO, BOFFETTA, GUIDO, MURATORE-GINANNESCHI, P & MUSACCHIO, STEFANO 2015 Dimensional transition of energy cascades in stably stratified forced thin fluid layers. *Physics of Fluids* **27** (3).
- TABELING, PATRICK 2002 Two-dimensional turbulence: a physicist approach. *Physics reports* **362** (1), 1–62.
- TRAN, CHUONG V 2004 Nonlinear transfer and spectral distribution of energy in α turbulence. *Physica D: Nonlinear Phenomena* **191** (1-2), 137–155.
- WATANABE, TAKESHI & IWAYAMA, TAKAHIRO 2004a Unified scaling theory for local and non-local transfers in generalized two-dimensional turbulence. *Journal of the Physical Society of Japan* **73** (12), 3319–3330.
- WATANABE, TAKESHI & IWAYAMA, TAKAHIRO 2004b Unified scaling theory for local and non-local transfers in generalized two-dimensional turbulence. *Journal of the Physical Society of Japan* **73**, 3319–3330.
- WATANABE, TAKESHI & IWAYAMA, TAKAHIRO 2007 Interacting scales and triad enstrophy transfers in generalized two-dimensional turbulence. *Physical Review E - Statistical, Nonlinear, and Soft Matter Physics* **76**.

- XIA, HUA, BYRNE, DAVID, FALKOVICH, GREGORY & SHATS, MICHAEL 2011 Upscale energy transfer in thick turbulent fluid layers. *Nature Physics* **7** (4), 321–324.
- YOUNG, ROLAND MB & READ, PETER L 2017 Forward and inverse kinetic energy cascades in jupiter’s turbulent weather layer. *Nature Physics* **13** (11), 1135–1140.